GRANMA manuscript No.
(will be inserted by the editor)

Granular packings of cohesive elongated particles

R.C. Hidalgo[1], D. Kadau[2], T. Kanzaki[3] and H.J. Herrmann[2,4]

Abstract We report numerical results of effective attractive forces on the packing properties of two-dimensional elongated grains. In deposits of non-cohesive rods in 2D, the topology of the packing is mainly dominated by the formation of ordered structures of aligned rods. Elongated particles tend to align horizontally and the stress is mainly transmitted from top to bottom, revealing an asymmetric distribution of local stress. However, for deposits of cohesive particles, the preferred horizontal orientation disappears. Very elongated particles with strong attractive forces form extremely loose structures, characterized by an orientation distribution, which tends to a uniform behavior when increasing the Bond number. As a result of these changes, the pressure distribution in the deposits changes qualitatively. The isotropic part of the local stress is notably enhanced with respect to the deviatoric part, which is related to the gravity direction. Consequently, the lateral stress transmission is dominated by the enhanced disorder and leads to a faster pressure saturation with depth.

Key words. Granular matter, Molecular Dynamics, non-spherical particles Quicksand, Collapsible soil

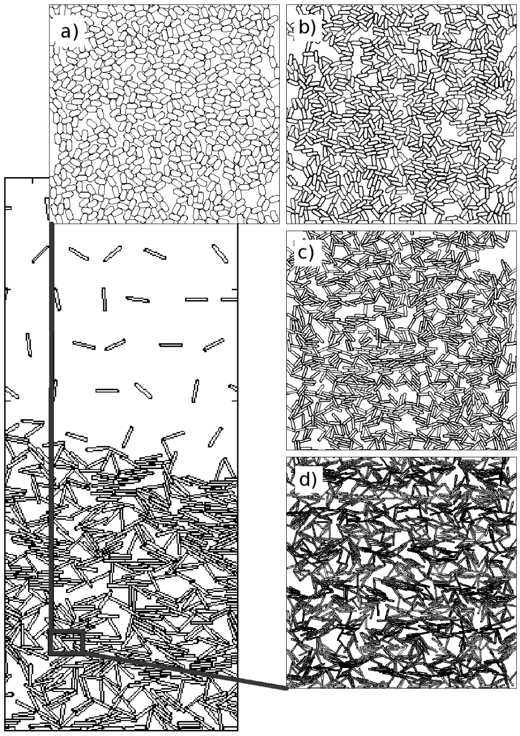

Fig. 1. Simulated packings of elongated cohesive particles settled by gravity. Final configurations are shown for the same granular bond number $Bo_g = 10^4$ and increasing elongation: (a) $d = 2$, (b) $d = 3$, (c) $d = 5$ and (d) $d = 10$.

1 Introduction

Nowadays, granular materials have remarkable relevance in engineering and physics [1,2,3]. During the last decades, important experimental and theoretical efforts have been made for better understanding the mechanical behavior of these many-body systems. Specifically, we highlight the career of **Professor Isaac Goldhirsch**, who has made a considerable number of remarkable contributions in this field [4,5,6,7,8].

Despite the fact that granular materials are often composed of particles with anisotropic shapes, like rice, lentils or pills, most of the experimental and theoretical studies have focused on spherical particles [1,2,3]. In recent years several studies have highlighted the qualitatively new features induced by particle shape [9,10,11,12,13,14,15,16,17,18]. These include effects in the packing fraction of granular piles [13,14], the pressure in the lateral walls of a silo during its discharge [15], the mean coordination num-

July 18, 2011

R.C. Hidalgo, D. Kadau, T. Kanzaki and H.J. Herrmann

Departamento de Física y Matemática Aplicada, Universidad de Navarra, 31080 Pamplona , Spain.
Departament de Física, Universitat de Girona, 17071 Girona, Spain
Institute for Building Materials, ETH Zürich, 8093 Zürich, Switzerland
Departamento de Física, Universidade Federal do Ceará, 60451-970 Fortaleza, Ceará, Brazil

Correspondence to: raul.cruz@udg.edu

ber [16], the jamming [17] and the stress propagation in granular piles [18]. Moreover, there is currently increasing interest on the effect that particle's shape has on the global behavior of granular materials [19,20,21,22,23,24].

Very often, loose and disordered granular structures appear in many technological processes and even everyday life. They can be found in collapsing soils [25,26,27, 28], fine powders [29,30,31] or complex fluids [32,33]. Generally, those fragile grain networks are correlated with the presence of cohesive forces [29,34,35,36]. Typical fine powders have in most cases an effective attractive force, e.g. due to a capillary bridge between the particles or van der Waals forces (important when going to very small grains, e.g. nano-particles). This force is known to be of great importance, e.g. for the mechanical behavior and the porosity of the macroscopic material [37,38,39,40]. This cohesive force leads also to the formation of loose and fragile granular packings as investigated in detail for structures generated by successive deposition of spherical grains under the effect of gravity [34,35,37,41].

The main objective of this work is to clarify the effect that an effective attractive force has on the packing properties of elongated grains. Here we focus on packings generated by deposition under gravity. The paper is organized as follows: in Section 2 we review the theoretical model used in the numerical simulations. The results on the deposit structure as well as the details of the packings' micro-mechanics are presented and discussed in Section 3. Finally, there is a summary with conclusions and perspectives.

2 Model

We have performed Discrete Element Modeling of a two-dimensional granular system composed of non-deformable oval particles, i.e. spheropolygons [10,11] composed of two lines of equal length and two half circles of same diameter. The width of a particle is the smaller diameter, given by the distance between the two lines (equals the circle diameter), whereas the length is the maximum extension. The aspect ratio d is defined by the length divided by width. This system is confined within a rectangular box of width W. Its lateral boundaries as well as the bottom are each built of one very long spheropolygonal particle, which is fixed. In order to generate analogous deposits, the system width is always set to $W = 20 \times d$ (in units of particle width). As illustrated in Fig. 1 the particles are continuously added at the top of the box with very low feed rate and a random initial velocity and orientation. The granular system settles under the effect of gravity and is relaxed until the particles' mean kinetic energy is several orders of magnitude smaller than its initial value.

In the simulation, each particle i ($i = 1...N$) has three degrees of freedom, two for the translational motion and one for the rotational one. The particles' motion is governed by Newton's equations of motion

$$m\ddot{\boldsymbol{r}}_i = \sum_j^c \boldsymbol{F}_{ij} - mg\ \hat{\boldsymbol{e}}_y, \qquad I\ddot{\theta}_i = \sum_j^c (\boldsymbol{l}_{ij} \times \boldsymbol{F}_{ij}) \cdot \hat{\boldsymbol{e}}_z, \quad (1)$$

where m is the mass of particle i, I its momentum of inertia, $\boldsymbol{r}_i$ its position and θ_i its rotation angle. g is the magnitude of the gravitational field and $\hat{\boldsymbol{e}}_y$ is the unit vector in the vertical direction. $\boldsymbol{l}_{ij}$ is the vector from the center of mass of particle i pointing to the contact point, $\hat{\boldsymbol{e}}_z$ is the normal vector in z-direction (perpendicular to the simulation plane). In Eq.1 $\boldsymbol{F}_{ij}$ accounts for the force exerted by particle j on i and it can be decomposed as $\boldsymbol{F}_{ij} = F_{ij}^N \cdot \hat{\boldsymbol{n}} + F_{ij}^T \cdot \hat{\boldsymbol{t}}$, where F_{ij}^N is the component in normal direction $\hat{\boldsymbol{n}}$ to the contact plane. Complementary, F_{ij}^T is the component acting in tangential direction $\hat{\boldsymbol{t}}$. For calculating the particles' interaction $\boldsymbol{F}_{ij}$ we use a very efficient algorithm proposed recently by Alonso-Marroquín et al [10,11], allowing for simulating a large number of particles. This numerical method is based on the concept of spheropolygons, where the interaction between two contacting particles only is governed by the overlap distance between them (see details in Ref. [10,11]). To define the normal interaction F_{ij}^N, we use a nonlinear Hertzian elastic force [43], proportional to the overlap distance δ of the particles. Moreover, to introduce dissipation, a velocity dependent viscous damping is assumed. Hence, the total normal force reads as $F_{ij}^N = -k^N \cdot \delta^{3/2} - \gamma^N \cdot v_{rel}^N$, where k^N is the spring constant in the normal direction, γ^N is the damping coefficient in the normal direction and v_{rel}^N is the normal relative velocity between i and j. The tangential force F_{ij}^T also contains an elastic term and a tangential frictional term accounting also for static friction between the grains. Taking into account Coulomb's friction law it reads as, $F_{ij}^T = \min\{-k^T \cdot \xi - \gamma^T \cdot |v_{rel}^T|,\ \mu F_{ij}^N\}$, where γ^T is the damping coefficient in tangential direction, v_{rel}^T is the tangential component of the relative contact velocity of the overlapping pair. ξ represents the elastic elongation of an imaginary spring with spring constant k^T at the contact [44], which increases as $d\xi(t)/dt = v_{rel}^T$ as long as there is an overlap between the interacting particles [44, 45]. μ is the friction coefficient of the particles.

Additionally, here we consider bonding between two particles in terms of a cohesion model with a constant attractive force F_c acting within a finite range d_c. Hence, it is expected that the density and the characteristics of the density profiles are determined by the ratio between the cohesive force F_c and gravity $F_g = mg$, typically defined as the granular Bond number $Bo_g = F_c/F_g$. Thus, the case of $Bo_g = 0$ corresponds to the cohesion-less case whereas for $Bo_g \to \infty$ gravity is negligible.

The equations of motion, Eqs.1, are integrated using a fifth order predictor-corrector algorithm with a numerical error proportional to $(\Delta t)^6$ [46], while the kinematic tangential displacement, is updated using an Euler's method. In order to model hard particles, the maximum overlap must always be much smaller than the particle size; this is ensured by introducing values for normal and tangen-

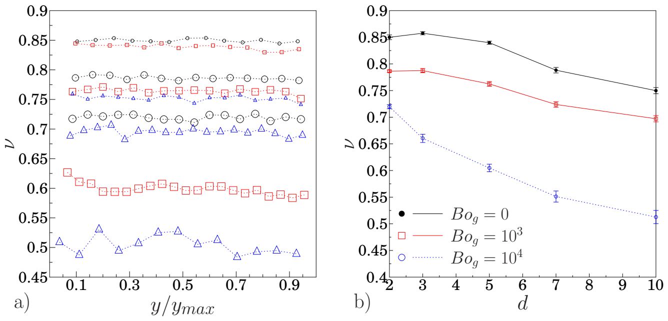

Fig. 2. (Color online) Density profiles of different granular deposits. In a) the circles represent particles with $d = 2$, the squares $d = 5$ and the triangles $d = 10$. The larger the symbols the stronger is the attractive force (small: $Bo_g = 0$; medium: $Bo_g = 10^3$; large: $Bo_g = 10^4$). In b) the evolution of the average volume fraction as a function of d is shown.

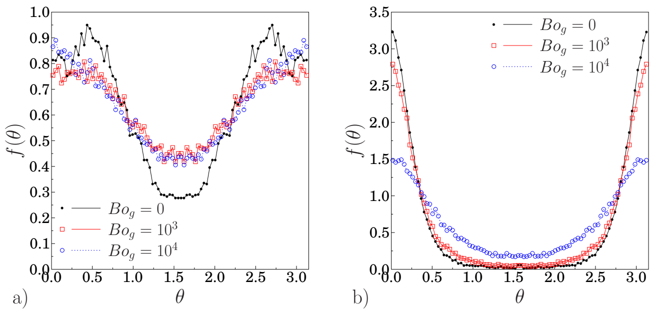

Fig. 3. Orientation distributions of particles for two aspect ratios, a) $d = 2$ and b) $d = 10$. In each case, results for several bond numbers are presented.

tial elastic constants, $k^T/k^N = 0.1$, $k^N = 10^3 N/m^{3/2}$. The ratio between normal and tangential damping coefficients is taken as $\gamma^N/\gamma^T = 3$, $\gamma^T = 1 \times 10^2 s^{-1}$ while gravity is set to $g = 10\ m/s^2$ and the cohesion range to $d_c = 0.0001$ (in units of particle width) to account for a very short range attraction, as mediated, e.g. by capillary bridges or van der Waals force. For these parameters, the time step should be around $\Delta t = 5 \times 10^{-6} s$. In all the simulations reported here, we have kept the previous set of parameters and only the particle aspect ratio and the Bond number Bo_g have been modified. We have also carried out additional runs (data not shown) using other particles' parameters, and we have verified that the trends and properties of the quantities we subsequently analyze are robust to such changes.

3 Results and discussion

We systematically study granular deposits of particles with aspect ratio from $d = 2$ to $d = 10$ and different Bond numbers. In all simulations presented here we have used 6×10^3 rods. In Fig. 1 we illustrate the granular packings obtained for several particle shapes and constant Bond number $Bo_g = 10^4$. Despite of the presence of a gravity field acting downwards, the formation of very loose and disordered granular structures is very noticeable. Moreover, as the aspect ratio of the particles increases, the volume fraction of the column decreases, showing a tendency to the formation of more disordered structures. This result contrasts with what was obtained for non-cohesive elongated particles. In that case, the topology of the packing is dominated by the face to face interaction and the formation of ordered structures of aligned rods is detected [47,23].

For better describing the packing structure, in Fig2a we present the density profiles depending on depth y/y_{max} obtained for several deposits of elongated particles. We plot for each particle aspect ratio density profiles with increasing strength of the attractive force illustrated in Fig2a by increasing symbol size. In systems composed by elongated particles with strong attractive forces the formation of extremely loose structures is observed, which are stabilized by the cohesive forces [41]. Moreover, in all cases the density profiles are quite uniform as function of depth. Typically, for the non-cohesive case a close packing is expected. For cohesive particles, smaller volume fraction values are found and the density profiles remain constant with depth. These density profiles have been studied and analyzed extensively for spherical particles [41] where constant density has been found only for fast deposition as strongly influenced by inertia. However, an extremely slow and gentle deposition process, allowing for relaxation of the deposit due to its own weight after each deposition, leads to a decreasing density with vertical position. Obviously, here the feed rate is not sufficiently slow. Additionally, as particles are added at the top they are accelerated before, thus reaching the deposit with a non negligible impact velocity.

Complementary, in Fig2b a systematic study of the global volume fraction depending on the particle aspect ratio is presented for different bond numbers. All curves show the overall trend of decreasing density with increasing aspect ratio d. For packings of non-cohesive particles disordered and thus substantially looser structures can only be found with very large aspect ratio as found earlier numerically and experimentally [23,24]. For very cohesive particles (see Fig.1), however, loose and disordered granular structures can be easily stabilized, leading to much lower densities independent on shape/elongation. This is notably enhanced as the aspect ratio of the particles increases and, consequently, the volume fraction of the packings quickly decreases.

In order to characterize the packing morphology, we examine the orientations of the particles. In figure 3, the distributions of particle's orientation $f(\theta)$, with respect to the horizontal direction, for rods with aspect ratio $d = 2$ and $d = 10$ are illustrated. We present results for several bond numbers. First, for the non-cohesive case, the

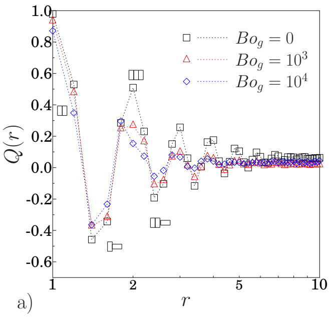

Fig. 4. (Color online) Radial orientation distribution functions, $Q(r)$, as defined in Eq. 2 for rod deposits with two different aspect ratios, a) $d = 2$ and b) $d = 5$. In each case, results for several Bond numbers are presented. At specific maxima/minima the corresponding particle configurations are illustrated.

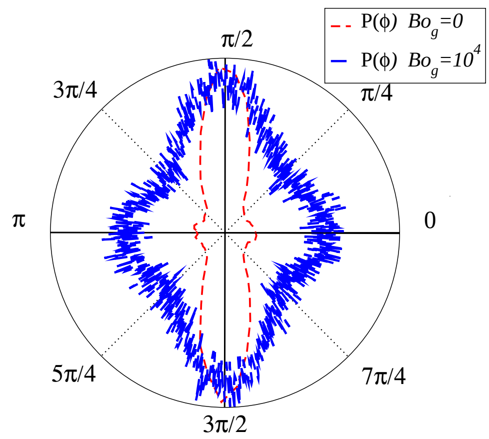

Fig. 5. (Color online) Polar distribution of the principal direction (larger eigenvalue of the stress tensor for each particle $\sigma_{\alpha\beta}$), obtained for particles with $d = 10$. For comparison, the data for $Bo_g = 0$ and $Bo_g = 10^4$ is presented.

geometry of the particle dominates the final structures of the compacted piles. Note that at the end of the deposition process, long particles ($d = 10$) most probably lie parallel to the substrate ($\theta = 0$ and $\theta = \pi$), while the most unlikely position corresponds to standing rods ($\theta = \frac{\pi}{2}$). Nevertheless, as the aspect ratio decreases, there is a shift in the most probable orientation, leading to a peaked distribution at an intermediate orientation [23,24]. Furthermore, this shift of the maximum is not observed for highly cohesive particles. In general, as the strength of the attractive force gets stronger, the final packing tends to a flatter distribution. As we pointed out earlier, very elongated particles with strong attractive forces form extremely loose structures. As the aspect ratio gets higher, the rods form highly jammed and disordered networks because during the deposition local particle rearrangements are constrained by the attractive force. The latter, is corroborated by the distribution of the angular orientation, where now the probability for standing rods which was zero in the non-cohesive case is enhanced with increasing bond number (fig. 3b). It seems that, for sufficiently large aspect ratio d, there is a threshold bond number needed to have a non-zero probability for standing rods.

The packing morphology is also examined through a radial orientation function $Q(r)$, defined as

$$Q(r) = \langle \cos\left(2(\theta_i - \theta_j)\right)\delta(\mathbf{r}_{ij} - r)\rangle \tag{2}$$

where θ_i and θ_j are the angular orientations of particles i and j, respectively. $Q(r)$ accounts for the mean value of the angular correlation between a given particle i and a particle j with their center of mass at a distance r_{ij}. Note that, this distribution function provides useful quantitative information on the local morphology of the rod packings. Configurations where the two rods are perpendicular to each other contribute -1 to $Q(r)$, while rods aligned along their long faces or along their short faces contribute with 1 [23,24].

In Fig4a and Fig4a the numerical data for packing of cohesive particles with aspect ratio $d = 2$ and $d = 5$ are shown for comparison. Both figures show a series of maxima (parallel alignment) and minima (perpendicular alignment), which develop at several distances. This correlates with the high tendency of the particles to align in closely packed structures, in particular for low attractive force strengths and the limiting case of non-cohesive particles [23,24]. As the strength of the interaction force gets larger looser structures are formed and consequently the intensity of the maxima and minima decreases. On the other hand, for very elongated particles (see Fig. 4.b) $Q(r)$ clearly indicates that the system does not show significant order. There is a maximum at contact, which simply indicates that at this shortest distance only perfectly aligned particles along their long faces can contribute. At larger distances a deep plateau seems to indicate a small preference at these intermediate distances to observed parallel aligned particles. Only a characteristic peak corresponding to the contact through the particle length $r = d$ seems to remain even for very strong attractive strengths. This picture suggests the lack of significant order and presence of strong density inhomogeneities, in granular deposits of very cohesive particles. As aspect ratio gets higher, this effect is notably enhanced.

Furthermore, we can correlate the microstructure with stress transmission by studying the micro-mechanical properties of the granular deposits. To this end, we introduce the stress tensor of a single particle i,

$$\sigma^i_{\alpha\beta} = \sum_{c=1}^{C_i} l^c_{i,\alpha} F^c_{i,\beta}, \tag{3}$$

which is defined in terms of the total contact force $\boldsymbol{F}^c_i$ that particle i experiences at contact c and the branch vector $\boldsymbol{l}^c_i$ related to the contact c. The sum runs over all the contacts C_i of particle i, α, β are the vectorial components.

In Figure 5, the polar distribution $P(\phi)$ of the principal direction ϕ related to the larger eigenvalue of $\sigma_{\alpha\beta}$,

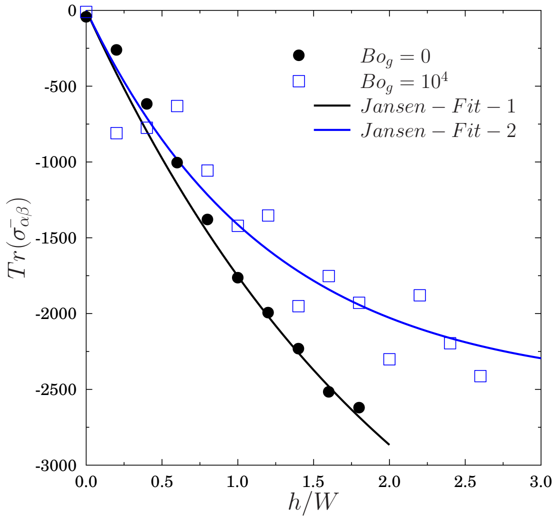

Fig. 6. Profiles of the trace of the mean stress tensor, obtained for particles with $d = 10$ and two different bond numbers. The depth is normalized with the width W of the system. We also show the fitting to the equation $\sigma = \sigma_m(1 - exp(-x/h_s))$, where we used $[\sigma_m = 2500N/m; h_s/W = 1.2]$ and $[\sigma_m = 4800N/m; h_s/W = 2.2]$ for case 1 and 2, respectively.

obtained for particles with aspect ratio $d = 10$ is illustrated. For the non-cohesive case ($Bo_g = 0$), Fig. 5 indicates that forces are preferentially transmitted in the vertical direction, displaying a high degree of alignment with the external gravity field. Note, that the stress is dominated by the contribution parallel to gravity (σ_{11}) whose mean value (data not shown) is also much higher than the stress in the horizontal direction (σ_{22}). For very cohesive particles (see Fig5), however, the polar distribution of the principal direction is more uniform, denoting the establishment of a more spherical stress state. Hence, in this case the stress is more isotropically transmitted while the alignment with the external gravity field diminishes. This effect correlates with the formation of very loose packings and the lack of significant order and the presence of strong density inhomogeneities.

Finally, we show that the changes in microstructure induced both by particle geometry and the attractive force lead to significant modifications in the pressure (trace of the mean stress tensor) profiles as a function of the silo depth h. The mean stress tensor, $\bar{\sigma}_{\alpha\beta}$, can be calculated for a given representative volume element (RVE) with area A_{RVE} resulting in

$$\bar{\sigma}_{\alpha\beta} = \frac{1}{A_{\mathrm{RVE}}} \sum_{i=1}^{N} w_v \sigma^i_{\alpha\beta}. \qquad (4)$$

The sum runs over the representative volume element while w_v is an appropriate average weight. Although recently Professor Isaac Goldhirsch and coworkers have developed a very accurate procedure for calculating w_v and $\bar{\sigma}_{\alpha\beta}$ [7,8], for simplicity's sake we use particle-center averaging and choose the simplest weighting: $w_v = 1$ if the center of the particle lies inside the averaging area A_{RVE} and $w_v = 0$ otherwise [48,49].

In Fig. 6, we display the trace of the mean stress tensor, defined following Eq. 4, for elongated particles with $d = 10$. For the calculation of the mean stress tensor we have used a representative volume element with a size equivalent to five particle lengths $A_{\mathrm{RVE}} = 5d \times 5d$. The depth has been normalized with the width of the deposit $x = h/W$. Moreover, for comparison, the numerical fit using a *Janssen-type* formula $\sigma = \sigma_m(1 - exp(-x/h_s))$, are also shown. Here, the magnitude of σ_m represents the saturation stress and h_s indicates the characteristic value of depth at which the pressure in the deposit stabilizes. As we have mentioned earlier, non-cohesive elongated particles transmit stress preferentially parallel to gravity. As a result, the weak transmission to the the lateral walls weakens pressure saturation (Fig. 6), which is reflected by the large saturation depth h_s and stress σ_m. The latter is consequence of the horizontal alignment of the flat faces of the rods, which induces an anisotropic stress transmission, from top to bottom. However, the scenario changes drastically for very cohesive particles. As we also pointed out earlier, when the attractive force is increased, particle orientations deviate from the horizontal and a larger disorder in the particle orientation distribution shows up. As a result, the spherical component of the local stress is notably enhanced with respect to the deviatoric part, which is related to the gravity direction. Hence, for very cohesive particles $B_o = 10^4$ of $d = 10$ we found notably smaller values of saturation depth h_s and stress σ_m. In this respect, introducing an attractive force has a very similar effect as reducing the particle elongation.

4 Conclusion

We have shown that introducing an attractive force in deposits of elongated grains has a profound effect on the deposit morphology and its stress profiles. In deposits of non-cohesive particles the topology is dominated by the formation of ordered structures of aligned rods. Elongated particles tend to align horizontally and the stress is mainly transmitted from top to bottom, revealing an asymmetric distribution of the local stress. Lateral force transmission becomes less favored compared to vertical transfer, thus hindering pressure saturation with depth. For deposits of cohesive particles, the preferred horizontal orientation is less pronounced with increasing cohesion. Very elongated particles with strong attractive forces form extremely loose structures, characterized by orientation distributions, which tend to a uniform behavior when increasing the Bond number. As a result of these changes, the pressure distribution in the deposits changes qualitatively. The spherical component of the local stress is notably enhanced with respect to the deviatoric part. Hence, the lateral stress transmission is promoted by the enhanced disorder and it leads to a faster pressure saturation with depth.

Acknowledgment

The Spanish MICINN Project FIS2008-06034-C02-02 has supported this work. This work started while the author RCH was visiting the IfB at the Eidgenössische Technische Hochschule of Zürich. Its financial support and hospitality are gratefully acknowledged. TK acknowledge the University of Girona (Spain) for financial support.

References

1. T. Pöschel, T. Schwager, Computational Granular Dynamics (Springer-Verlag Berlin Heidelberg New York, 2005).
2. H.M. Jaeger, S.R. Nagel, R.P. Behringer, *Rev. Mod. Phys.* **68**, 1259 (1996).
3. I.S. Aranson, L.S. Tsimring, *Rev. Mod. Phys.* **78**, 641 (2006).
4. I. Goldhirsch, *Annual Review of Fluid Mechanics* **35**, 267-293 (2003).
5. C. Goldenberg, I. Goldhirsch, *Nature* **435**, 188-191 (2005).
6. C. Goldenberg, I. Goldhirsch *Phys. Rev. Lett.* **89**, 084302 (2002).
7. C. Goldenberg, A.P.F. Atman, P. Claudin, G. Combe, I. Goldhirsch, *Phys. Rev. Lett.* **96**, 168001 (2006).
8. I. Goldhirsch, C. Goldenberg, *Eur. Phys. J. E* **9**, 245-251 (2002).
9. J.A.C. Gallas, S. Sokolowski, *International Journal of Modern Physics B* **7**, 2037-2046 (1993).
10. F. Alonso-Marroquín, H.B. Muhlhaus, H.J. Hermann, *Particuology* **6**, 390-403 (2008).
11. F. Alonso-Marroquín, Y. Wang, *Granular Matter* **11**, 317-329 (2009).
12. S.A. Galindo-Torres, F. Alonso-Marroquín, Y.C. Wang, D. Pedroso, J.D. Muñoz Castaño, *Phys. Rev. E* **79**, 060301 (2009).
13. F.X. Villarruel, B.E. Lauderdale, D.M. Mueth, H.M. Jaeger, *Phys. Rev. E* **61**, 6914 (2000).
14. A. Donev, I. Cisse, D.Sachs, E.A. Variano, F.H. Stillinger, R. Connelly, S. Torquato, P.M. Chaikin, *Science* **303**, 990 (2004).
15. Z. Zhong, J.Y. Ooi and J.M. Rotter, *Eng. Struct.* **23**, 756-767 (2001).
16. J. Blouwolff, S. Fraden, *Europhys. Lett.* **76**, 1095 (2006).
17. K. Desmond, S.V. Franklin, *Phys. Rev. E.* **73**, 031306 (2006); M. Trepanier, S.V. Franklin, *Phys. Rev. E* **82**, 011308 (2010).
18. I. Zuriguel, T. Mullin, J.M. Rotter, *Phys. Rev. Lett.* **98**, 028001 (2007); I. Zuriguel, T. Mullin, *Proc. Roy. Soc. A* **464**, 99 (2008).
19. G. Lumay, N.Vandewalle, *Phys. Rev. E* **70**, 051314 (2004); G. Lumay, N. Vandewalle, *Phys. Rev. E* **74**, 021301 (2006).
20. E. Azéma, F. Radjai, R. Peyroux, *Phys. Rev. E* **76**, 011301 (2007).
21. E. Azéma, F. Radjai, G. Saussine, *Mechanics of Materials* **41**, 729-741 (2009).
22. E. Azéma, F. Radjai, *Phys. Rev. E* **81**, 051304 (2010).
23. R.C. Hidalgo, I. Zuriguel, D. Maza, I. Pagonabarraga, *Phys. Rev. Lett.* **103**, 118001 (2009).
24. R.C Hidalgo, I. Zuriguel, D. Maza, I. Pagonabarraga, *J. Stat. Mech.* P06025 (2010); T. Kanzaki, R.C. Hidalgo, D. Maza, I. Pagonabarraga, *J. Stat. Mech.* P06020 (2010).
25. J. Mitchell, K. Soga, Fundamentals of soil behavior (Wiley-New Jersey, 2005).
26. L. Barden, A. McGown, K. Collins, *Engineering Geology* **7**, 49 (1973).
27. A. Assallay, C. Rogers, I. Smalley, *Engineering Geology* **48**, 101 (1997).
28. Y. Reznik, *Eng. Geol.* **78**, 95 (2005).
29. P.G. Rognon, J.-N. Roux, D.E. Wolf, M. Naaïm, F. Chevoir, *Europhysics Letters* **74**, 644 (2006).
30. D. Kadau, L. Brendel, G. Bartels, D.E. Wolf, M. Morgeneyer, J. Schwedes, *Chemical Engineering Transactions* **3**, 979 (2003).
31. M. Roeck, M. Morgeneyer, J. Schwedes, D. Kadau, L. Brendel, D.E. Wolf, *Granular Matter* **10**, 285293 (2008).
32. N.J. Wagner, J.F. Brady, *Physics Today* **62**, 27 (2009).
33. E.D. Gado, W. Kob, *Soft Matter* **6**, 1547 (2010).
34. D. Kadau, H.J Herrmann, J. Andrade Jr., A. Araújo, L. Bezerra, L. Maia, *Brief Communications to Granular Matter* **11**, 67 (2009).
35. D. Kadau, H.J. Herrmann, J. Andrade, *Eur. Phys. J. E* **30**, 275 (2009).
36. D. Kadau, in *Powders and Grains 2009*, AIP Conference Proceedings **1145**, 981-984, Eds M. Nakagawa and S. Luding, Amer. Inst. Physics (2009).
37. D. Kadau, in *IUTAM-ISIMM Symposium on Mathematical Modeling and Physical Instances of Granular Flows*, AIP Conference Proceedings **1227**, 50-57, Eds J.D. Goddard and J.T. Jenkins, Amer. Inst. Physics (2010).
38. D. Kadau, G. Bartels, L. Brendel, and D.E. Wolf, *Phase Transit.* **76**, 315 (2003).
39. D. Kadau, G. Bartels, L. Brendel, D.E. Wolf, *Comp. Phys.Comm* **147**, 190 (2002).
40. G. Bartels, T. Unger, D. Kadau, D. Wolf, J.Kertész, *Granular Matter* **7**, 139 (2005).
41. D. Kadau, H.J. Herrmann, *Physical Review E* **83**, 031301 (2011).
42. C. Nouguier-Lehon, B. Cambou, E. Vincens, *Int. J. Numer. Anal. Meth. Geomech.* **27**, 1207-1226 (2003).
43. L.D. Landau, E.M. Lifshitz, Theory of Elasticity (Butterworth-Heinemann, 1986).
44. P.A. Cundall, O.D.L. Strack, *Géotechnique* **29**, 47 (1979).
45. G. Duvaut, J.-L. Lions, Les Inéquations en Mécanique et en Physique (Dunod, Paris, 1972).
46. M. P. Allen, D. J. Tildesley, Computer Simulation of Liquids (Clarendon Press, Oxford, 1987).
47. O. Ditlevsen, K.N. Berntsen, *Journal of Engineering Mechanics, ASCE* **5**, 561-569 (1999).
48. M. Lätzel, S. Luding, H.J. Herrmann, *Granular Matter* **2**, 123 (2000).
49. M. Madadi, O. Tsoungui, M. Lätzel, S. Luding, *Int. J. Sol. Struct.* **41**, 2563-2580, (2004).